Journal of Solid State Chemistry 182 (2009) 1944–1949

Contents lists available at ScienceDirect

Journal of Solid State Chemistry

journal homepage: www.elsevier.com/locate/jssc

Structural characterization and electrical properties of $NiNb_{2-x}Ta_xO_6$ ($0 \le x \le 2$) and some Ti-substituted derivatives

M. López-Blanco, U. Amador, F. García-Alvarado *

Departamento de Química, Universidad San Pablo-CEU, Urbanización Montepríncipe, 28668 Boadilla del Monte, Madrid, Spain

ARTICLE INFO

Article history:
Received 2 January 2009
Received in revised form
2 April 2009
Accepted 28 April 2009
Available online 13 May 2009

Keywords:
Columbite
Rutile
Electrical properties
Structural characterization

ABSTRACT

A structural and electrical characterization of the system $NiNb_{2-x}Ta_xO_6$ ($0 \le x \le 2$) is presented. For $x \le 0.25$ materials with the columbite-type structure typical of $NiNb_2O_6$ have been obtained whereas for $x \ge 1$ tri-rutile-like oxides were obtained. The electrical properties are similar in both cases; they are semiconducting with very low electrical conductivity and very high activation energy, though slight differences were found as a function of Ta content. Improvement of conductivity by reducing the stoichiometric materials could not be achieved due to decomposition. In this connection, partial substitution of Nb or Ta by Ti has been carried out in order to create oxygen vacancies. Tantalum was partially replaced by Ti to a significant extent in the tri-rutile structure inducing a slight increasing of conductivity. However, for the columbite case neither Nb nor Ta could be partially replaced. This behavior is quite different from that reported for other similar columbites such as $MnNb_2O_{6-\delta}$, which exhibits high electrical conductivity upon substitution of niobium by titanium.

1. Introduction

AB_2O_6 (columbite/tri-rutile) type of oxides where B is either Nb or Ta are very interesting materials that have been investigated in view of their dielectric properties and uses in a wide range of related applications [1–5]. Besides, some of them have been proposed as water splitting photocatalyst [6–8] as it is the case of NiM_2O_6 (M = Nb, Ta). When M = Nb the oxide crystallizes in the columbite structure whereas for M = Ta a tri-rutile-like material is formed. To our best knowledge, the solubility range of both phases is not known; therefore, we have first investigated the phases present in the system $NiNb_2O_6$–$NiTa_2O_6$. Since the columbite and tri-rutile structures are closely related [9] some degree of solubility could be expected. One of the common features in both structures is that MO_6 octahedrons share edges which makes more difficult the formation of oxygen vacancies when compared to corner-sharing based structures (the perovskite for instance). However, we have recently shown that a Nb-based columbite, $MnNb_2O_6$, can be modified by either reduction or substitution in the Nb site, to yield good electronic conductors [10,11]. Even more, oxygen ion conductivity has been detected. These results on columbites are interesting because oxides presenting both electronic and oxygen ion conductivity may be useful as highly efficient electrodes in solid oxide fuel cells. In the case of the columbite $MnNb_2O_{6-\delta}$ [10], it was found that the quantity of oxygen vacancies that can be created is small ($\delta \sim 0.02$). As a novelty it was also found that $MnNb_2O_6$ is affected by an intrinsic instability and instead of the nominal composition two close phases with either lower or higher Mn contents may stabilize. The formation of the latter, $Mn_{1.1}Nb_{1.9}O_6$, is possible because to the oxidation of Mn(II) to Mn(III). Interestingly, when Nb(V) is partially replaced by Ti(IV) this charge-compensating mechanism also operates [11]. The presence of trivalent manganese is responsible of the p-type electronic conductivity observed at ambient pO_2. However, at much lower pO_2, Mn(III) is reduced and electrical conductivity decreases; further reduction affects Nb(V) or Ti(IV) and n-type conductivity is then observed. Oxygen ion conductivity in this material is low since in the best case a value of $6.0 \times 10^{-5}\,\Omega^{-1}\,cm^{-1}$ at 900°C was found.

In the present paper we present the behavior of another member of the columbite family, $NiNb_2O_6$, for which oxidation of the divalent metal, Ni(II), at ambient pO_2 is not likely to occur. On the other hand, we have replaced Nb by Ta to study the series $NiNb_{2-x}Ta_xO_6$ for which the limit members are the columbite $NiNb_2O_6$ [12,13] and the tri-rutile $NiTa_2O_6$ [14], similarly to what occurs for $FeNb_{2-x}Ta_xO_6$ [15]. We aimed to analyze the effects of aliovalent substitution in the pentavalent site of columbite and tri-rutile looking for an improvement of electrical conductivity. In particular, we have replaced Ti^{4+} by either Nb^{5+} or Ta^{5+}, similarly to what was made in the case of $MnNb_2O_6$ for which an increasing of electrical conductivity by several orders of magnitude was achieved [11].

* Corresponding author.
E-mail address: flaga@ceu.es (F. García-Alvarado).

0022-4596/$ - see front matter © 2009 Elsevier Inc. All rights reserved.
doi:10.1016/j.jssc.2009.04.038

2. Experimental

The synthesis of oxides with nominal composition $NiNb_{2-x}Ta_xO_6$ ($0 \le x \le 2$) was carried out at high temperature by reaction of stoichiometric mixtures of Nb_2O_5 (99.99%), Ta_2O_5 (99.99%) and $Ni(NO_3)_2 \times H_2O$ (20.43% in Ni). First, the blends were heated at 800 °C for 12 h to fully decompose the nitrate; afterwards, they were ground, pelletized and heated up again at temperatures ranging from 1250 °C (for $x = 0$) to 1300 °C (for $x = 1$). Pellets were slowly cooled down to 800 °C and finally quenched in air from that temperature. The same procedure was followed to obtain the Ti-substituted derivatives: $NiNb_{2-y}Ti_yO_6$ and $NiNb_{1.75}Ta_{0.25-y}Ti_yO_6$ ($y = 0.1$, 0.15) and $NiNb_{0.25}Ta_{1.75-y}Ti_yO_6$ ($y = 0.15$ and 0.30).

Structural characterization of the samples was performed by powder X-ray diffraction (XRD) on a Bruker D8 high-resolution diffractometer using a monochromatic Cu$K\alpha_1$ ($\lambda = 1.5406$ Å) radiation obtained with a germanium primary monochromator; diffracted beams were recorded using a position-sensitive detector (PSD) MBraun PSD-50 M. Diffraction patterns were analyzed by the Rietveld method using the program FullProf [16].

Energy dispersive spectroscopy (EDS) has been carried out on a Scanning Electron Microscope JEOL JSM 6400 equipped with an OXFORD INCA EDS detector. Several spectra were recorded in order to analyze the homogeneity of the samples and the eventual presence of different types of particles. This equipment was also used to analyze the morphology on as-prepared pellets obtained by the sintering process described below.

Magnetic susceptibility measurements were made using a SQUID magnetometer (Quantum Design, model MPMS-XL). The temperature dependence of magnetization (M) was measured in the temperature range 2–300 K at an applied magnetic field (H) of 0.1 T upon heating samples under zero-field-cooled conditions from 2 K (previously cooled at $H = 0$ T). The experimental molar magnetic susceptibility χ_{exp} (M/H) was calculated on the basis of the sample mass and the molecular weight. The molar paramagnetic susceptibility χ_m was then obtained by subtraction of the diamagnetic contribution from each ion.

Electrical characterization has been performed by impedance spectroscopy (IS) using a FRA Solartron 1260 coupled with a 1290 Dielectric Interface in the 1 MHz–0.1 Hz range in the temperature interval 25–800 °C. Measurements were carried out on pellets whose polished faces were coated with platinum which acts as electrodes.

To get dense pellets, powdery samples were mixed with polyvinyl alcohol, as a binder, compacted into pellets and heated up to 800 °C very slowly (2 °C/min) to decompose the binder. Afterwards, pellets were fired at the synthesis temperature (1250–1300 °C) or slightly above it and slowly cooled down to 800 °C before being quenched in air. The density of pellets was measured by the Archimedes method. Relative densities were find to be the same (approximately 88%) for the whole composition range explored, $NiNb_{2-x}Ta_xO_6$ ($0 \le x \le 2$). On the other hand sintered Ti-substituted samples were found to have relative densities higher than 95%.

3. Results and discussion

Samples $NiNb_{2-x}Ta_xO_6$ with $x = 0$, 0.25, 0.5, 0.75, 1, 1.25, 1.5, 1.75 and 2 have been prepared. The columbite structure has a narrow existence range since only the samples with $x = 0$ and 0.25 were found to be single-phase exhibiting this structure. Fig. 1a shows the XRD pattern for $NiNb_{1.75}Ta_{0.25}O_6$; all the diffraction peaks can be interpreted with the cell and symmetry of columbite [13]. On the other hand, single-phase samples with tri-rutile structure were found for $x = 1$, 1.5, 1.75 and 2. As an example, Fig. 1b shows the XRD pattern for $NiNb_{0.25}Ta_{1.75}O_6$; all the Bragg peaks can be assigned to cells similar to that one of the tri-rutile $NiTa_2O_6$ [14]. On the other hand, for $x = 0.75$ tri-rutile is the main phase but an unidentified second phase is present. This suggests that, in the phase-diagram, the stability region of tri-rutile starts somewhere between $x = 0.75$ and 1. Cell volume per

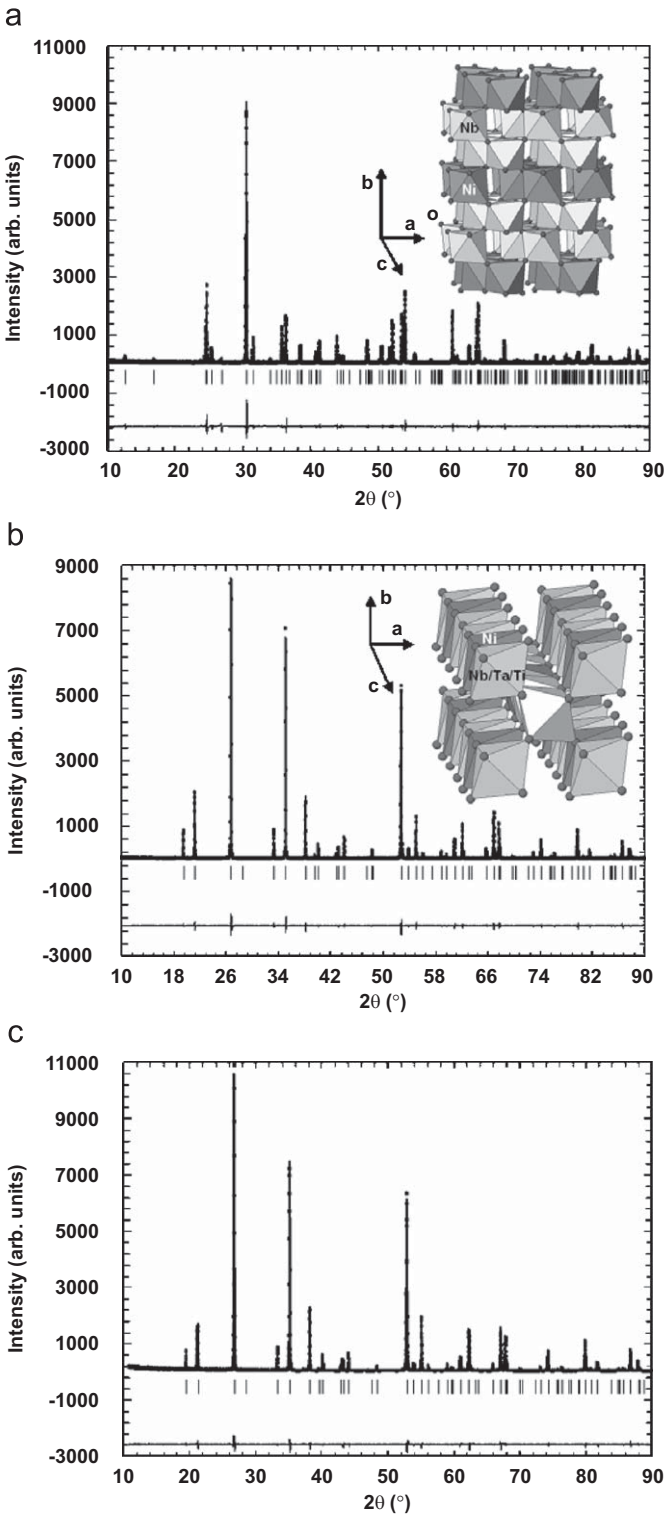

Fig. 1. Experimental X-ray diffraction patterns and calculated (profile matching) of (a) $NiNb_{1.75}Ta_{0.25}O_6$ (columbite), (b) $NiNb_{0.25}Ta_{1.75}O_6$ (tri-rutile) and (c) $NiNb_{0.25}Ta_{1.45}Ti_{0.30}O_{6-\delta}$ (tri-rutile). The insets show schematic representations of columbite (a) and tri-rutile (b).

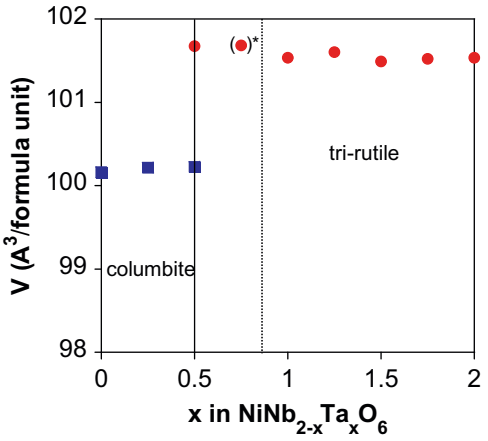

Fig. 2. Cell volume per formula unit as a function of tantalum content. ($Z_{columbite} = 4$ f.u./unit cell, $Z_{tri\text{-}rutile} = 2$ f.u./unit cell). The asterisk indicates the presence of a minor second phase for this composition. Dashed vertical line between $x = 0.75$ and 1 indicates that somewhere between these two compositions the tri-rutile single-phase region starts.

Table 1
Lattice parameters for tri-rutile $NiNb_{0.25}Ta_{1.75}O_6$ and some Ti-substituted samples.

Nominal composition	a (Å)	c (Å)	v (Å^3)
$NiNb_{0.25}Ta_{1.75}O_6$	4.7184(1)	9.1205(1)	203.05(1)
$NiNb_{0.25}Ta_{1.6}Ti_{0.15}O_{5.925}$	4.7127(1)	9.1163(3)	202.47(1)
$NiNb_{0.25}Ta_{1.45}Ti_{0.3}O_{5.85}$	4.7055(5)	9.1091(5)	201.69(3)

formula unit for each composition is graphically presented in Fig. 2; the variation for each phase is within the experimental error, indicating that the cell-volume does not change when Nb/Ta ratio does. This agrees with the fact that the ionic radii of both Nb(V) and Ta(V) are the same (0.64 Å in octahedral coordination [17]).

Regarding the Ti-substituted derivatives, the tri-rutile $NiNb_{0.25}Ta_{1.75-y}Ti_yO_6$ accepts the partial replacement of Ta by Ti; both $y = 0.15$ and 0.30 samples have been found to be single-phase as it is shown for example in Fig. 1c. Beyond $y = 0.3$ secondary phases have detected. Lattice parameters decrease as Ti replaces Ta, as it can be seen in Table 1. This variation is expected taking into account the ionic radii of Ta(V) and Ti(IV) (0.64 and 0.605 Å, respectively, in octahedral coordination [17]). Interestingly, it has not been possible to replace either Nb or Ta by Ti in the columbites $NiNb_2O_6$ and $NiNb_{1.75}Ta_{0.25}O_6$ even though synthesis of samples with small amount of Ti ($y < 0.15$) were also attempted. Therefore, for $NiNb_2O_6$ a behavior different from the one observed in the case $MnNb_2O_6$ [11] has been found. A tentative explanation of this difference is given below.

Fig. 3 shows representative scanning micrographs of the faces of sintered pellets with nominal composition $NiNb_{2-x}Ta_xO_6$ $x = 0.25$ (columbite), $x = 1.75$ (tri-rutile) and $NiNb_{0.25}Ta_{1.60}Ti_{0.15}O_6$ (tri-rutile). A significant difference can be seen in particle size. In the former (Fig. 3a) particle size is larger than for the tantalum-rich tri-rutile (Fig. 3b). However, we have not found any influence of particle size in the sintering process since all samples sintered to 88% relative density. A better sintering of the tri-rutiles has been obtained after partial substitution of Ta by Ti. For $NiNb_{0.25}Ta_{1.60}Ti_{0.15}O_{6-\delta}$ a relative density of 95% has been reached. The corresponding SEM image (Fig. 3c) shows a typical image of high dense ceramics. On the other hand, the metallic ratios determined by EDS in all the samples are in agreement with the corresponding nominal compositions. For example, for

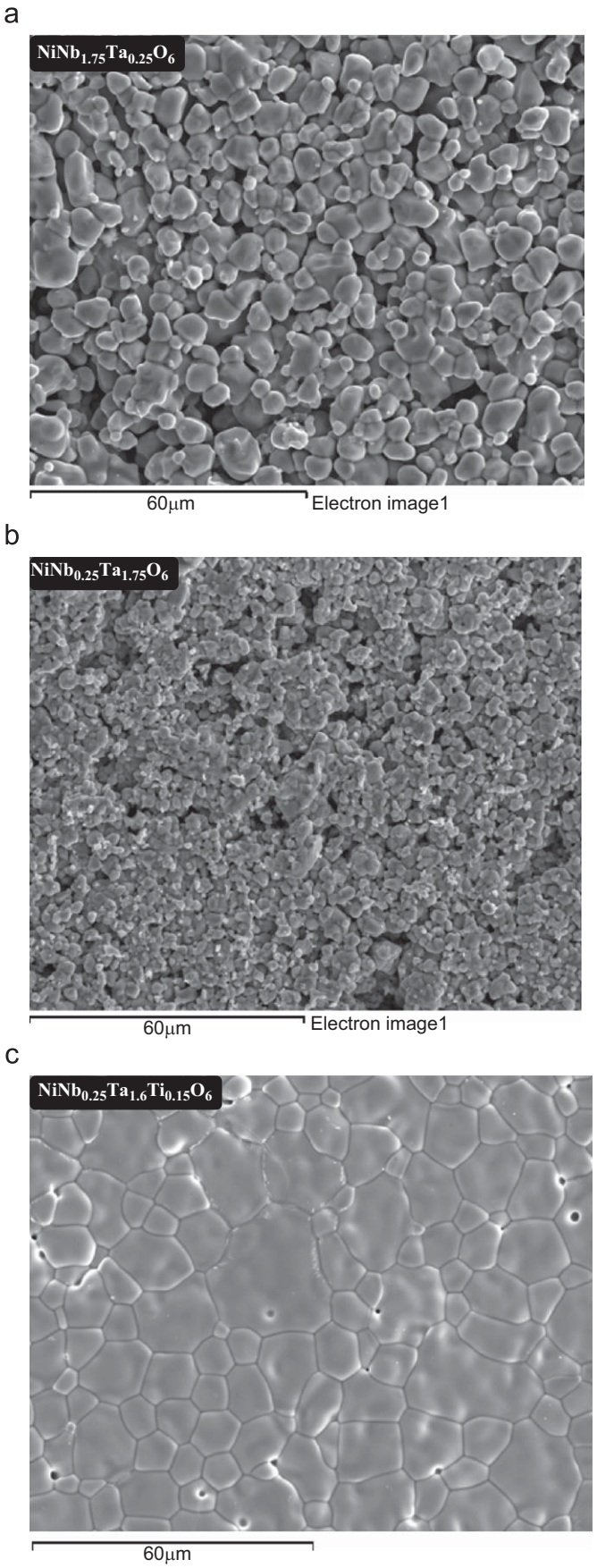

Fig. 3. SEM images of pellet face of (a) $NiNb_{1.75}Ta_{0.25}O_6$ sintered at 1250 °C, (b) $NiNb_{0.25}Ta_{1.75}O_6$ sintered at 1300 °C and (c) $NiNb_{0.25}Ta_{1.6}Ti_{0.15}O_{6-\delta}$ sintered at 1300 °C.

nominal $NiNb_{1.75}Ta_{0.25}O_6$, the formula estimated by EDS is $NiNb_{1.72(2)}Ta_{0.28(1)}O_6$ assuming an oxygen content close to the ideal stoichiometry.

Fig. 4a shows a typical Nyquist plot depicting the electrical response of $NiNb_{2-x}Ta_xO_6$ with $x=0$ in the temperature range 550–840 °C. For $x=0.25$ the same characteristics are found in the corresponding plot. The spectra were fitted to equivalent circuits comprising a resistor in parallel with a constant phase element that are in series with another similar parallel combination. At lower temperature only the high frequency semicircle (see Fig. 4b) is detected. Besides, it can be seen that the real part of impedance is zero at the highest frequency reached in the experiment. Above 840 °C only the low frequency semicircle is detected. In such cases only total conductivity could be obtained from fitting. Constant phase elements (CPE) were used instead of pure capacitor due to the slight depression observed in the semicircles. In particular, this is significant in the low frequency semicircle. The capacitance values associated to the semicircles have been obtained from the relationship $C=R^{(1-n)/n}Q^{1/n}$, where R is the resistance, Q is the pseudo capacitance of the CPE and n indicates the degree of deviation with respect to the value of the pure capacitor. As an example, in the case of $NiNb_2O_6$ the corresponding capacitance values obtained for the high and the low frequency semicircles are 2.3×10^{-12} and 7.8×10^{-9} F cm^{-1}, respectively. Consequently, the high frequency semicircle is assigned to the response of the bulk resistance whereas the low frequency semicircle is assigned to the grain boundary response. The corresponding values obtained for $NiNb_{2-x}Ta_xO_6$ with $x=0.25$ are similar. Fig. 5a shows the Arrhenius behavior of the bulk conductivity for both samples, $x=0$ and 0.25. It can be seen that increasing the Ta content in the columbite side of the system $NiNb_2O_6$–$NiTa_2O_6$ has a slight deleterious effect on the bulk conductivity. For $x=0.25$ conductivity is as low as $10^{-5}\,\Omega^{-1}\,cm^{-1}\,K^{-1}$ at 800°C; besides, the activation energies are very high (ca. 1.3 eV). On the other hand, grain boundaries seem to be more sensitive to Ta substitution in the columbite-like materials as it can be seen in Fig. 5b.

Low conductivities and high activation energies are also found for $NiNb_{2-x}Ta_xO_6$ with $x=1$, 1.5, 1.75 and 2.0, all of them exhibiting a tri-rutile-like structure. From the corresponding Nyquist plots (see for example Fig. 6) capacitances and resistances are extracted for the different observed phenomena. Thus, high-frequency semicircles are assigned to the bulk response in view of their capacitances (for example 3.12×10^{-12} F cm^{-1} in the case of $NiNb_{0.5}Ta_{1.5}O_6$). The low frequency semicircles could be only reliably fitted in some cases for which capacities ca. 10^{-9} F cm^{-1} were calculated. These values suggest that this semicircle is due to grain boundaries response. The Arrhenius behavior of the bulks are shown in Fig. 7 for two selected samples ($x=1.5$ and 2.0). It can be seen that conductivity is very low and activation energies are very high (greater than 1 eV in all cases). On the other hand, poor information was obtained for

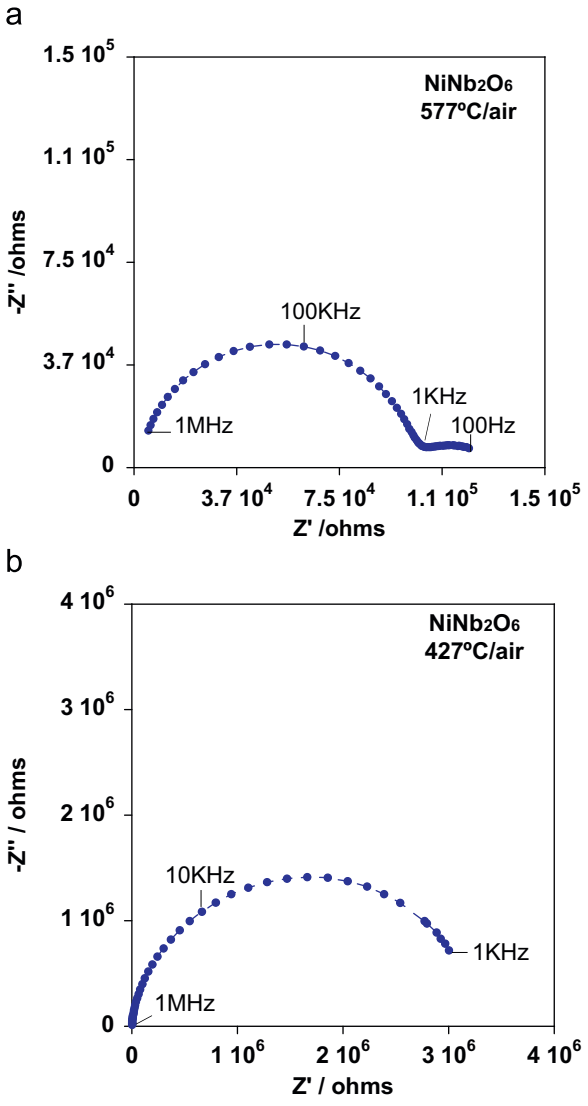

Fig. 4. Impedance data presented in the Z''–Z' plane for pelletized $NiNb_2O_6$ sintered at 1250 °C. Spectrum recorded at (a) 577 °C and (b) 427 °C.

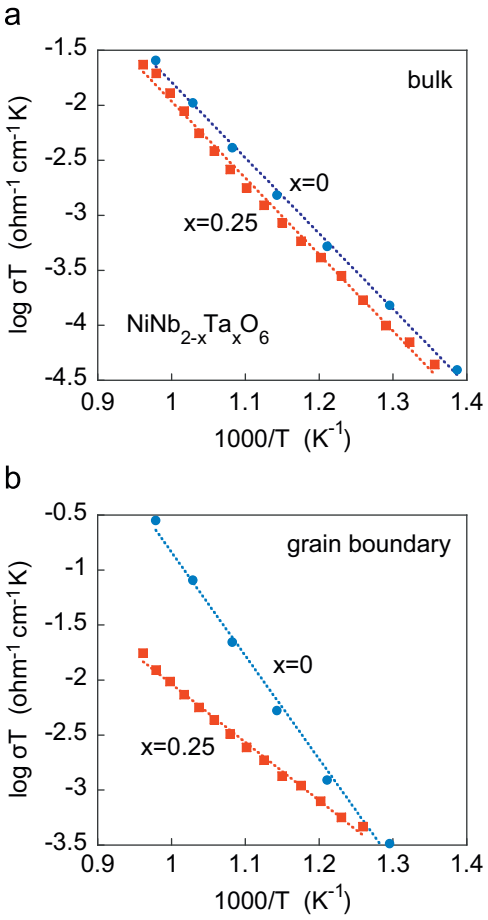

Fig. 5. Arrhenius plot showing the temperature dependence of conductivity of $NiNb_{2-x}Ta_xO_6$ ($x=0$ and 0.25): (a) bulk and (b) grain boundary.

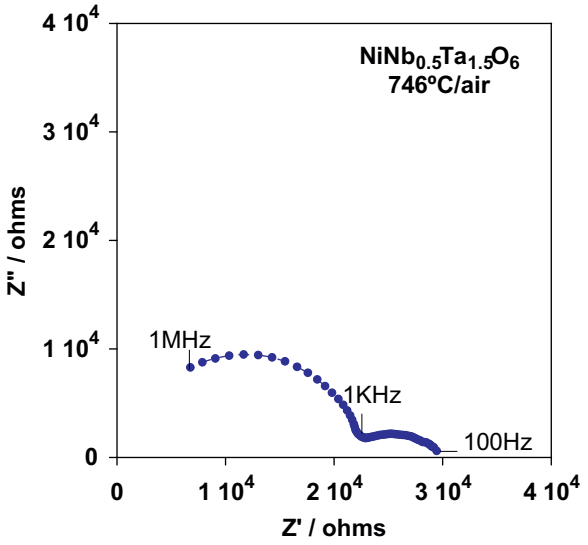

Fig. 6. Impedance data presented in the Z″–Z′ plane for pelletized $NiNb_{0.5}Ta_{1.5}O_6$ sintered at 1300 °C. The spectrum shown was recorded at 746 °C.

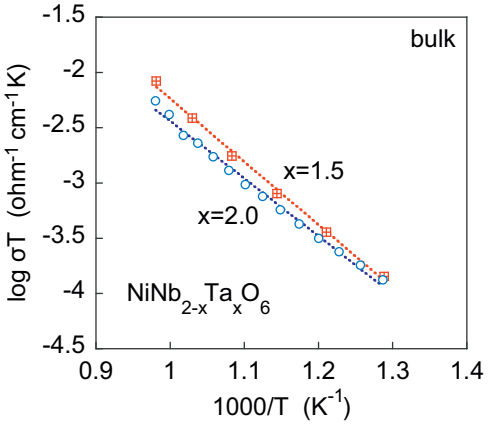

Fig. 7. Arrhenius plot showing the temperature dependence of bulk conductivity of $NiNb_{2-x}Ta_xO_6$ ($x = 1.5$ and 2).

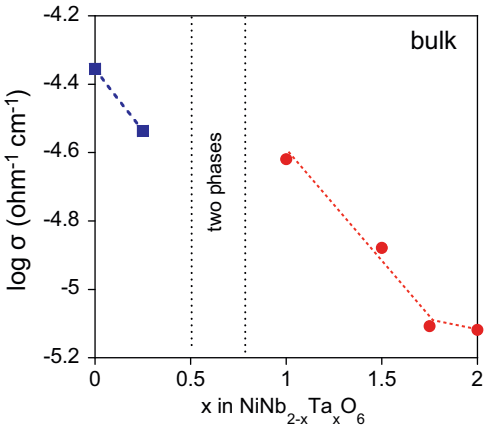

Fig. 8. Bulk conductivity of $NiNb_{2-x}Ta_xO_6$ ($0 \le x \le 2$) as a function of tantalum content.

the dependence of grain boundary with temperature due to the flat response obtained in most of cases.

Fig. 8 shows the variation of bulk conductivity with the Ta content for the whole series. The observed trend is that the higher the Ta content is, the lower the conductivity found, though it is quite low in all cases. To explain this we have thought firstly of the origin of electrical conductivity in $NiNb_2O_6$. Besides intrinsic defects, the semiconducting behavior of the columbite $NiNb_2O_6$ may be due to the slight reduction of Nb(V) at high temperature. This may also explain the high activation energy observed. The reduction process is expected to become more difficult if it is Ta(V) the cation that has to be reduced, explaining the dependence of conductivity with the Ta content (see Fig. 8).

In other related Nb-based columbites and rutiles conductivity increases when Nb(V) ions are partially reduced to Nb(IV) ions as it has been observed for $MnNb_2O_6$ and $CrNbO_4$ [10,18]. In these cases, electronic conductivity changes by several orders of magnitude because electrons are injected in the conduction band upon reduction. Similarly, we tried to improve the electronic conductivity of materials in the system $NiNb_{2-x}Ta_xO_6$ by reducing these oxides under 5% H_2/Ar at 1100 °C. However, they decomposed under this reducing atmosphere to form metallic Ni and some other phases. Another possible approach to improve the electrical conductivity of $NiNb_{2-x}Ta_xO_6$ may be to replace Nb(V) by Ti(IV). Upon substitution two charge compensating mechanisms could operate: oxidation of Ni^{2+} to Ni^{3+} and loss of oxygen. The former would produce holes and the latter oxygen vacancies. Note that in the case of $MnNb_{2-x}Ti_xO_{6-\delta}$ both charge carriers contribute to an increase of conductivity of several orders of magnitude [11]. Therefore, the substitution of either Ta(V) or Nb(V) by Ti(IV) have been tried in some members of the $NiNb_{2-x}Ta_xO_6$ series.

In the case of the columbite-like oxides ($x = 0$ and 0.25) substitution of Ta by Ti has not been achieved in the temperature range attempted in the synthesis process (up to 1400 °C). A comparison to the case of $MnNb_{2-x}Ti_xO_{6-\delta}$ ($x_{max} = 0.02$) sheds some light about the immiscibility of TiO_2 and $NiNb_2O_6$. When Nb is replaced by Ti in $NiNb_2O_6$ both of the above mentioned charge-compensating mechanisms might operate. However, oxidation of Ni(II) to Ni(III) is not likely to occur as easy as oxidation of Mn(II) to Mn(III) (the case of $MnNb_2O_6$). Thus, the formation of oxygen vacancies would be the only way to balance the loss of positive charge. The example of $MnNb_2O_6$ gives again an idea of the readiness of Nb-columbites to lose oxygen. The maximum value of δ in $MnNb_2O_{6-\delta}$ has been found to be ca. 0.02 when prepared at 1150 °C under Ar/H_2 (95:5) [10]. Therefore, if inducing oxygen vacancies in $NiNb_2O_6$ is also difficult, none of the two possible charge-compensating mechanisms is likely to favor substitution of Nb(V) by Ti(IV) and hence the reaction does not take place.

In the case of tri-rutiles, the sample $NiNb_{0.25}Ta_{1.75}O_6$ was selected to replace Ta by Ti. Substitution took place up to a very high extent: $NiNb_{0.25}Ta_{1.75-y}Ti_yO_6$ ($y_{max} = 0.3$). Note that in this case the structure seems to be more suited to accept oxygen vacancies, as we have already found for reduced $CrNbO_4$ [18] with rutile-like structure.

To determine the actual charge-compensating mechanism operating these tri-rutile-like oxides upon Ti-doping we looked for an evidence of the oxidation state of nickel by analyzing the magnetic behavior of both $NiNb_{0.25}Ta_{1.75}O_6$ and $NiNb_{0.25}Ta_{1.45}Ti_{0.3}O_{6-\delta}$. The effective magnetic moment of $NiNb_{0.25}Ta_{1.75}O_6$ at room temperature is 3.2μ_B which is within the usual range for Ni^{2+} [19] if one takes into account that incomplete quenching of the orbital momentum of Ni^{2+} electrons is found very often in nickel oxides [20,21]. On the other hand, the effective magnetic moment for $NiNb_{0.25}Ta_{1.45}Ti_{0.3}O_{6-\delta}$ is only slightly higher, 3.4μ_B, indicating that if high-spin Ni^{3+} has formed upon substitution its amount is very small. Therefore, the main charge compensating mechanism proposed is the formation of anion vacancies.

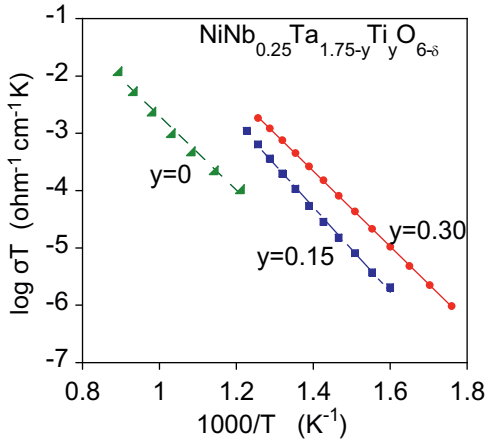

Fig. 9. Arrhenius plot showing the temperature dependence of total conductivity of $NiNb_{0.25}Ta_{1.75-y}Ta_yO_{6-\delta}$ ($y = 0$, 0.15 and 0.30).

Although substitution produces a beneficial effect on sinterization, the electrical measurements did not allow a deep analysis of bulk and grain boundary conductivities because the different electrical responses could not be separated. Typical Nyquist (not shown) present two overlapped semicircles that could not be resolved. Therefore, only total conductivity for some selected temperatures were determined. Nevertheless, the obtained results deserve some comments. Fig. 9 shows the Arrhenius behavior of $NiNb_{0.25}Ta_{1.75-y}Ti_yO_{6-\delta}$ with $y = 0$, 0.15 and 0.30 and $\delta \sim y/2$; it can be seen that conductivity increases upon substitution albeit it remains low. For example, the conductivity at 800 °C for the parent ($y = 0$) material is $5 \times 10^{-6}\,\Omega^{-1}\,cm^{-1}$ whereas for $y = 0.30$ it increases up to $3 \times 10^{-4}\,\Omega^{-1}\,cm^{-1}$.

It is likely that the difficulty to oxidize Ni(II) to Ni(III) is at the origin of the low conductivity observed. Note that for $MnNb_2O_6$ the oxidation of Mn(II) to Mn(III) upon substitution increases conductivity by four orders of magnitude whereas conductivity of $NiNb_{0.25}Ta_{1.75-y}Ti_yO_{6-\delta}$ is no more than two orders larger than that of $NiNb_{0.25}Ta_{1.75}O_6$. Therefore, the change of conductivity in the substituted tri-rutiles may be due to both the presence of oxygen-vacancies and the beneficial effect of Ti on sintering.

4. Conclusions

The existence range of both columbite and tri-rutile in the series $NiNb_{2-x}Ta_xO_6$ has been determined. The columbite-type structure typical of $NiNb_2O_6$ has been obtained for $x \leq 0.25$. On the other hand, for $1 \leq x \leq 2$ the tri-rutile-type structure of $NiTa_2O_6$ was obtained.

The electrical properties of both columbites and tri-rutiles are similar as they are semiconducting with very low electrical conductivity and very high activation energy. Small differences were found as a function of Ta content. In any case it seems that Ta has a deleterious effect likely due to the high stability of the pentavalent state. Improvement of conductivity by reduction of $NiNb_{2-x}Ta_xO_6$ could not be achieved due to decomposition. In this connection, creation of oxygen vacancies were tried by partial substitution of Nb(V) or Ta(V) by Ti(IV). Tantalum was partially replaced by Ti to a significant extent in the tri-rutile-like materials inducing an increasing of conductivity of almost two orders of magnitude. However, neither Nb nor Ta could be partially replaced in the columbites samples. This behavior is different from that reported for other similar columbites, such as $MnNb_2O_{6-\delta}$, that exhibited high electrical conductivity upon substitution. In $MnNb_2O_6$ oxidation of Mn(II) to Mn(III) provides holes that improve conductivity by four orders of magnitude. On the contrary, for the Ni-based columbites and tri-rutiles herein investigated it seems that the main charge compensating mechanism is the formation of oxygen vacancies. This operates effectively in the Ti-substituted tri-rutiles, as for example $NiNb_{0.25}Ta_{1.75-y}Ti_yO_{6-\delta}$. The values of conductivity in these materials suggest that the contribution to total electrical conductivity of oxygen-vacancies in edge-sharing structures can be noticeable. However, in the present case the contribution could not be quantified as Ti also benefits the sintering process likely reducing the grain boundary resistance significantly.

Acknowledgments

We thank "Ministerio de Ciencia e Innovación" and "Comunidad de Madrid" for funding the projects MAT2007-64486-C07-01 and S-0505/PPQ/0358, respectively. Financial support from Universidad San Pablo CEU is also acknowledged. European Commission has partially funded a grant for M. López-Blanco through the ESF. Finally, we are also indebted to J. Romero (UCM) for magnetic measurements.

References

[1] M. Thirumal, A.K. Ganguli, Proceedings of the Indian Academy of Sciences—Chemical Sciences 113 (2001) 603–610.
[2] M. Thirumal, I.N. Jawahar, K.P. Surendiran, P. Mohanan, A.K. Ganguli, Materials Research Bulletin 37 (2002) PII S0025-5408(0001)00812-00811.
[3] M. Thirumal, A.K. Ganguli, Progress in Crystal Growth and Characterization of Materials 44 (2002) PII S0960-8974(0902)00011-00016.
[4] M. Thirumal, A.K. Ganguli, Materials Research Bulletin 36 (2001) 2421–2427.
[5] H.J. Lee, K.S. Hong, S.J. Kim, I.T. Kim, Materials Research Bulletin 32 (1997) 847–855.
[6] L. Guochang, L. Peraldo Bicelli, G. Razzini, Borromei, Materials of Chemistry and Physics 23 (1989) 477–490.
[7] K. Kunimori, H. Oyanagi, H. Shindo, Catalysis Letters 21 (1993) 283–290.
[8] J.H. Ye, Z.G. Zou, A. Matsushita, International Journal of Hydrogen Energy 28 (2003) PII S0360-3199(0302)00158-00151.
[9] A.F. Wells, Structural Inorganic Chemistry, fifth ed., Clarendon Press, Oxford, 1984.
[10] F. Garcia-Alvarado, A. Orera, J. Canales-Vazquez, J.T.S. Irvine, Chemistry of Materials 18 (2006) 3827–3834.
[11] A. Orera, F. Garcia-Alvarado, J.T.S. Irvine, Chemistry of Materials 19 (2007) 2310–2315.
[12] R. Wichmann, H. Mullerbuschbaum, Zeitschrift Fur Anorganische Und Allgemeine Chemie 503 (1983) 101–105.
[13] H. Weitzel, Zeitschrift Fur Kristallographie 144 (1976) 238–258.
[14] H. Mullerbuschbaum, R. Wichmann, Zeitschrift Fur Anorganische Und Allgemeine Chemie 536 (1986) 15–23.
[15] C.A. Dossantos, J. Deoliveira, Solid State Communications 82 (1992) 89–91.
[16] J. Rodriguez-Carvajal, in: Fullprof, Satellite Meeting on Powder Diffraction of the XV Congress of the IUCr, Toulouse, France, 1990.
[17] R.D. Shannon, Acta Crystallographica Section A 32 (1976) 751–767.
[18] J.C. Perez-Flores, F. Garcia-Alvarado, Solid State Sciences 11 (2009) 207–213.
[19] R. Valenzuela, Magnetic Ceramics, Cambridge University Press, Cambridge, 1994.
[20] H.B.G. Casimir, J. Smit, U. Enz, J.F. Fast, H.P.J. Wijn, E.W. Gorter, A.J.W. Duyvesteyn, J.D. Fast, J.J. Dejong, Journal De Physique Et Le Radium 20 (1959) 360–373.
[21] J.M. Hastings, L.M. Corliss, Reviews of Modern Physics 25 (1953) 114–121.